Statistical modeling of transspectral processes in laser sensing of the environment. 1. Raman scattering

G.M. Krekov and M.M. Krekova

Institute of Atmospheric Optics,
Siberian Branch of the Russian Academy of Sciences, Tomsk

Received June 30, 2004

Peculiarities of statistical modeling of the transspectral processes used in laser sensing of meteorological parameters of the atmosphere are analyzed. The necessity of using rigorous Monte Carlo technique appears in the case of operation of the corresponding meteorological lidars under cloudy conditions in the atmosphere, when the contribution of multiply scattered radiation to lidar return signal becomes significant. Principal attention in this paper is paid to peculiarities of constructing the algorithms for modeling the processes of the radiation transfer. An important role of the proper choice of the model of elastic and inelastic scattering is demonstrated. In particular, when modeling the angles of photon scattering in the process of the Markov wandering, the scattering phase function shape must be chosen adequate to conditions of the Raman excitation. Results of methodical calculations are presented in comparison with data of other authors. Based on the results obtained, some peculiarities in the formation of multiple scattering background in the Raman sensing channels have been found.

Introduction

Remote laser sounding is now one of the methods providing prompt information about violation of normal operation of an ecological system. Traditional laser sounding technique is based on interpretation of spatially resolved signal of elastic scattering from the medium under study at one or several frequencies in the optical wavelength range.[1] The regular tendency has been formed in recent decade of using a wide spectrum of linear and nonlinear processes resulting in re-emission of radiation by the matter of the medium under study at another frequencies, the so-called transspectral proceses.[2,3] The phenomena of spontaneous Raman scattering[4–6] and laser-induced fluorescence[6,7] are the most significant among the linear processes, which will be considered in this paper. One relates some perspectives with the use of Brillouin molecular scattering[8] and hyper-Rayleigh scattering.[9] The account for Ring effect[10] and resonance Raman scattering[6] is important in the systems of passive optical sounding including the operated orbital systems ENVISAT, etc.

In the first part of the paper, we concentrate our attention on the analysis of potential capabilities of the optical laser radars (Raman lidars) intended for use in sounding the atmosphere. The Raman lidar, when being effectively used, is capable of obtaining regular data on the spatial distribution of the majority of the basic parameters of the atmosphere necessary for analysis and forecast of the state of the air basin up to the level of cirrus clouds.

Results of systematic observations have been accumulated and analyzed in the frameworks of the European aerosol lidar network (EARLINET)[11] and Siberian Lidar Station.[12] These results are related, first of all, to the study of long-term time series of the vertical profiles of humidity, temperature, and ozone concentration. Analysis of these data allows one to judge on the effect of the dynamics of strong atmospheric fronts,[13] emissions of volcanic eruptions,[14] emissions of industrial origin,[15] and other anomalous impacts destroying equilibrium of the ecological system.

Combination of the Raman lidar with multifrequency elastic scattering lidars[16,17] allows obtaining data on the vertical variations of microstructure of atmospheric aerosol of both background and anthropogenic origin. A particular class of the inverse problems of optical sounding of the atmosphere arises at Raman diagnostics of the aforementioned parameters under conditions of cloudy atmosphere. Continuous cloudiness of lower level does not promise any success in application of lidars for this purpose. At the same time, optically thin cirrus clouds are the subjects of increasing interest of specialists in the field of both passive and active sounding.[18] The reason is that cirrus clouds, even invisible, play an important role in the formation of radiation budget of the planet[19] and, on the other hand, they are the source of active interference for spaceborne optical sounding tools.

Method of solution

Correct statement of the direct problem of lidar sounding implies solving non-stationary radiation transfer equation under complicated boundary conditions representing real experiment. The Boltzmann equation for the radiation transfer process including inelastic scattering takes the form:

0235-6880/04/10 745-08 $02.00

$$c^{-1}\frac{\partial I(\mathbf{r},\mathbf{\Omega},t,\lambda)}{\partial t}+\mathbf{\Omega}\nabla I(\mathbf{r},\mathbf{\Omega},t,\lambda)=-\sigma(\mathbf{r},\lambda)I(\mathbf{r},\mathbf{\Omega},t,\lambda)+$$

$$+1/4\pi\int_L\int_{4\pi}G(\mathbf{r},\mathbf{\Omega}',\mathbf{\Omega},\lambda')I(\mathbf{r},\mathbf{\Omega}',t,\lambda')\mathrm{d}\Omega'\mathrm{d}\lambda'+S(\mathbf{r},\mathbf{\Omega},\lambda); \quad (1)$$

$$G(\mathbf{r},\mathbf{\Omega}',\mathbf{\Omega},\lambda')=G_{\mathrm{M}}(\mathbf{r},\mathbf{\Omega}',\mathbf{\Omega},\lambda'=\lambda)+$$
$$+\int_L G_{\mathrm{R}}(\mathbf{r},\mathbf{\Omega}',\mathbf{\Omega},\lambda')\,\mathrm{d}\lambda', \quad (2)$$

where $S(\mathbf{r},\mathbf{\Omega},\lambda)$ is the source function, $I(\mathbf{r}, \Omega, t, \lambda) = I(x)$ is the intensity at the wavelength λ at the point $\mathbf{r}$ in the direction Ω at the time moment t; $x = (\mathbf{r}, \mathbf{\Omega}, t, \lambda)$ is the point of the phase space $x \in X$,

$$X=\{(\mathbf{r},\mathbf{\Omega},t,\lambda):\mathbf{r}\in Q\subset R^3,\ \mathbf{\Omega}\in W=$$
$$=\{(a,b,c)\in R^3:a^2+b^2+c^2=1\},\ t\in T,\lambda\in L\}$$

or $X = Q \times W \times T \times \Lambda$ is the eight-dimension phase space; $G_{\mathrm{M}}(\mathbf{r}, \mathbf{\Omega}, \mathbf{\Omega}', \lambda)$ is the volume coefficient of the directed elastic light scattering, mainly the Mie scattering, in the direction $(\mathbf{\Omega}, \mathbf{\Omega}')$; $G_{\mathrm{R}}(\mathbf{r}, \mathbf{\Omega}, \mathbf{\Omega}', \lambda')$ is the volume coefficient of the directed inelastic scattering (Raman in this case) of the photon with the wavelength λ' accompanied by the transspectral transition $(\lambda' \to \lambda)$; $\sigma(\mathbf{r}, \lambda)$ is the total extinction coefficient at the wavelength λ, i.e.

$$\sigma(\mathbf{r},\lambda)=\sigma_{\mathrm{a}}(\mathbf{r},\lambda)+\sigma_{\mathrm{S}}(\mathbf{r},\lambda)+\sigma_{\mathrm{R}}(\mathbf{r},\lambda'\to\lambda), \quad (3)$$

where $\sigma_{\mathrm{a}}(\mathbf{r}, \lambda)$ is the absorption coefficient of the disperse medium, $\sigma_{\mathrm{S}}(\mathbf{r}, \lambda)$ and $\sigma_{\mathrm{R}}(\mathbf{r}, \lambda)$ are, respectively, the scattering coefficients of elastic and inelastic interaction. Usually in scalar case G_{M} and G_{R} depend only on the scattering angle ϑ between the directions Ω' and Ω, i.e., $\vartheta = (\mathbf{\Omega}', \mathbf{\Omega})$.

The radiation transfer equation (1) is written in the scalar approximation, i.e. without the account of polarization effects. Nevertheless, its accurate analytic solution has not yet been reached. The Monte Carlo method[21] is the most rational among the numerical methods. Although this method does not require accurate form of the transfer equation,[22] construction of the effective weight algorithms of the method[23] is based on transformations of the integral transfer equation adequate to the initial problem. Transformation of the Eq. (1) containing the spectral dependence of the functionals to be estimated in the integral form, is presented, for example, in Ref. 23. It is shown that it keeps its canonic form of the 2nd-kind Fredholm equation:

$$f(x)=\int_X k(x',x)f(x')\mathrm{d}x'+\psi(x) \quad (4)$$

or

$$f=Kf+\psi, \quad (5)$$

$$f(x)=\sigma(x)I(x) \quad (6)$$

and means the density of the photon collisions. Then, in Eq. (4)

$$k(x',x)=\frac{\Lambda(\mathbf{r}',\lambda)g(\mu,\mathbf{r}',\lambda)\exp\left[-\tau(\mathbf{r}',\mathbf{r},\lambda)\right]}{2\pi|\mathbf{r}-\mathbf{r}'|}\times$$
$$\times\delta\left(\mathbf{\Omega}-\frac{\mathbf{r}-\mathbf{r}'}{|\mathbf{r}-\mathbf{r}'|}\right)\delta\left[t'-t+\left(\frac{|\mathbf{r}'-\mathbf{r}|}{c}\right)\right], \quad (7)$$

where

$$\Lambda(\mathbf{r}',\lambda)=\left[\sigma_{\mathrm{S}}(\mathbf{r}',\lambda)+\sigma_{\mathrm{R}}(\mathbf{r}',\lambda\to\lambda')\right]/\sigma(\mathbf{r}',\lambda)$$

is the single scattering albedo, and

$$g(\mu,\mathbf{r}',\lambda)=\frac{\sigma_{\mathrm{S}}(\mathbf{r}',\lambda)g_{\mathrm{M}}(\mu,\mathbf{r}',\lambda)+\sigma_{\mathrm{R}}(\mathbf{r}',\lambda)g_{\mathrm{R}}(\mu,\mathbf{r}',\lambda)}{\sigma(\mathbf{r}',\lambda)}$$

is the mean weighted scattering phase function; $\mu = \cos(\vartheta)$; g_{M} and g_{R} are scattering phase functions of the elastic and inelastic scattering normalized to unit;

$$\tau(\mathbf{r}',\mathbf{r};\lambda)=\int_0^l\sigma(\lambda,\mathbf{r},l')\mathrm{d}l'$$

is the optical length of the segment $l = |\mathbf{r}' - \mathbf{r}|$;

$$\psi(x)=p(\mathbf{r}_0)p(\mathbf{\Omega}_0)p(t_0)p(\lambda_0)$$

is the multiplicative density of the external sources, where $p(m_0)$ are the partial densities of the corresponding initial coordinates m_0; naturally

$$\int_R p(m_0)\mathrm{d}m=1.$$

Rationality of the Monte-Carlo method lies in the fact that it allows obtaining the estimate of both radiation fluxes and linear functionals of the form

$$I_\lambda=(f,\varphi)=\int_{D\subset X}f(x)\varphi(x)\mathrm{d}x \quad (8)$$

over a preset domain of the phase space $D \subset X$, ($\varphi(x)$ is the characteristic function). Integration over the variables in Eq. (7) is realized during modeling, that essentially optimizes the calculation process. The index λ in Eq. (8) shows that the spectral behavior of the backscattered signal in the area of hypothetic detector is of interest for this problem. It is impossible to detect insignificant variations of the signal δI_λ within the limits of a fine spectral structures of Raman scattering in the frame of analog modeling. In such cases one should use one of the weight methods[22,24] related to the correlated sample (method of independent tests).[22] Briefly, the idea of the method is as follows.

Let the kernel of the integral equation (4) and the functions ψ, φ depend on some parameter, the wavelength λ in the case under consideration. Then, following Ref. 22, we have for the statistical estimate of the functional

$$\hat{I}_\lambda = (f_\lambda, \varphi_\lambda) = M\sum_{n=1}^{N} Q_n(\lambda)\varphi(x_n, \lambda), \qquad (9)$$

where $\{x_n\}$ is the physical chain of collisions, Q_n is the statistical weight of the photon, M is the sign of mathematical expectation. After each transition $x' \to x$ the weight of the particle at some basic wavelength λ_0 is transformed to another wavelength λ or the set of wavelengths by the formula

$$Q(\lambda_j) = Q(\lambda_0)\frac{k_{\lambda_j}(x', x)}{k_{\lambda_0}(x', x)}. \qquad (10)$$

One can assume because of the relatively small length of the spectral interval including the Raman scattering lines, that the spectral properties of the atmosphere are determined only by the behavior of $\sigma(\lambda)$, $G(\lambda) = G(\lambda_0)$. Then the transformation (10) is essentially simplified:

$$Q(\lambda_j) = Q(\lambda_0)\frac{\sigma(\mathbf{r}, \lambda_j)}{\sigma(\mathbf{r}, \lambda_0)}\exp\left[-\left(\tau(\mathbf{r}, \mathbf{r}', \lambda) - \tau(\mathbf{r}, \mathbf{r}', \lambda_j)\right)\right]. \qquad (11)$$

Another one weight method determining the basis of the whole algorithm is the method of "local estimate" in the version formulated in Ref. 25. The estimate of the Raman-lidar return intensity, as it follows from statistical modeling, is

$$I_{i,k}(\lambda) = 1/c\Delta t_k \int\limits_{\Delta\mathbf{r}^*}\int\limits_{\Delta\Omega_i^*}\int\limits_{\Delta t_k} I(\mathbf{r}, \mathbf{\Omega}, t, \lambda)\mathrm{d}\mathbf{r}\mathrm{d}\mathbf{\Omega}\mathrm{d}t \qquad (12)$$

in the vicinity of a given detector D. The detector is determined by the set of the field-of-view angles $\Delta\mathbf{\Omega}_i^* = \sin\vartheta_\mathrm{d}^i \mathrm{d}\vartheta\mathrm{d}\varphi$, the spatial volume $\Delta\mathbf{r}^* = \pi R_\mathrm{d}$ and the grid of temporal resolution $\Delta l_k = \Delta t_k c$, where c is the light speed.

Model of the medium

Solution of the transfer equation is sought under the initial and boundary conditions corresponding to the optical arrangement of monostatic ground-based and spaceborne lidars. The satellite lidar is at the height $H_0 = 700$ km from the Earth's surface. It is assumed that the source emits a δ-pulse in the direction cone $2\pi(1 - \cos\varphi_i)$, where $\varphi_i = 0.2$ mrad is the total divergence angle of the source. The return optical signal is collected with a receiver in the angular cones $2\pi(1 - \cos\varphi_\mathrm{d}^i)$, where φ_d^i is the set of the total receiving angles: 0.2; 0.4; 0.6, and 1 mrad.

The optical characteristics of the atmosphere are the step functions of the height h. The atmosphere is divided into n_h homogeneous layers with the irregular step $\Delta h_i = h_{i+1} - h_i$, $i = 1, 2, \ldots, n_h$. The model values of the interaction coefficients and the scattering phase function are set in each layer Δh_i. The characteristics of the following types of interactions are included into the initial database under conditions of the cloudy atmosphere: molecular scattering (Cabannes–Rayleigh and Raman), aerosol absorption taking into account the single scattering albedo $\Lambda(h)$, aerosol scattering, and scattering on cloud droplets and crystals.

Modeling of the Raman scattering

From the standpoint of the molecular-statistic theory of light scattering,[26] there is no strictly coherent scattering in nature. Indeed, the so-called Rayleigh scattering is the sum of the rotational Raman spectral (RRS) lines and the central Cabannes line. The Cabannes line at fine spectral resolution and certain conditions of detection is divided to the Brillouin line doublet around the Landau-Placzek line. None of these processes is completely coherent. The diagram of the spectral structure of the molecular backscattering from the atmosphere is shown in Fig. 1. Nevertheless, let us assume in the numerical experiment that scattering in the generalized Cabannes line is coherent, and let us model the inelastic scattering in the vibrational-rotational Raman spectrum.

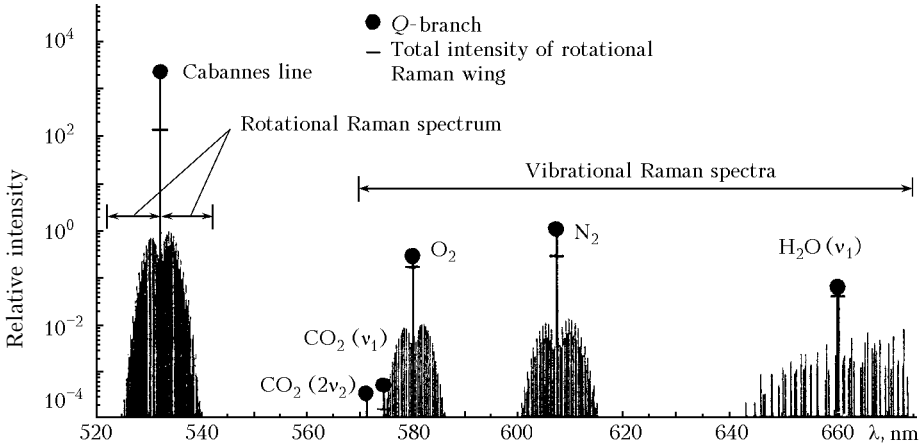

Fig. 1. Spectral structure of molecular backscattering of laser radiation at the wavelength $\lambda = 532$ nm, according to the data of Ref. 27. Intensity of the RRS lines is calculated for $T = 300$ K and the water vapor mixing ratio $\omega_{H_2O} = 1\%$.

First attempts of statistically modeling the rotational Raman scattering were undertaken by G. Kattavar et al.[28,29] in the problem of quantitative interpretation of so-called Ring effect. Following Ref. 29, let us assume that when a photon has undergone molecular scattering at the carrier frequency ν_0 at one of the stages of Markovian chain of collisions in a multi-component scattering medium, a part of its "weight," let it be q_0, remains in the limits of the Cabannes line. The rest, $1 - q_0$, weight goes to one of the frequencies ν' of the rotational or vibrational-rotational Raman spectrum (VRS). The intensity of radiation redistributed to the Raman frequencies depends on the mean polarizability of molecules α and the anisotropy of the polarizability δ.

For the diatomic molecules we have

$$q_0 = \frac{\left[180 + 13\varepsilon(\lambda)\right] + \left[180 + \varepsilon(\lambda)\right]\cos^2\vartheta}{\left[180 + 52\varepsilon(\lambda)\right] + \left[180 + 4\varepsilon(\lambda)\right]\cos^2\vartheta}, \quad (13)$$

where ϑ is the scattering angle, and $\varepsilon = (\delta/\alpha)^2$. As is shown,[30] the value $1 - q_0$ weakly changes along the spectrum for the molecules N_2 and O_2, and in the UV and near IR wavelength ranges it lies within the limits 0.035–0.025. In order to avoid unpleasant procedure of selecting the conditional density $p(q_0/\vartheta)$, one can use the method of statistical averaging[22] and take the mean value over a solid angle

$$\bar{q}_0 = (18 + \varepsilon)/(18 + 4\varepsilon). \quad (14)$$

As is known, the mean polarizability is determined as

$$|\bar{\alpha}|^2 = (n-1)^2 / 4\pi N_0^2, \quad (15)$$

where n is the refractive index, $N_0 = 2.687 \cdot 10^{15}$ cm^{-3} is the Loschmidt number. Thus, the intensities of the rotational Raman lines of N_2 and O_2 molecules are related by the following relationship:

$$I_R = \eta_{N_2} I_{N_2}^R + \eta_{O_2} I_{O_2}^R \frac{1 - q_{N_2}}{1 - q_{O_2}}, \quad (16)$$

where η_{N_2} and η_{O_2} are, respectively, the mixture ratio of nitrogen and oxygen in the atmosphere.

The relative intensity of lines of the normalized RRS is determined as[26]:

$$I_R(J,T) = \nu_J^4 q_J \frac{Bhc}{kT} b_{J\to J'} \exp(E_J / kT), \quad (17)$$

where J, J' are the rotational quantum numbers of the initial and final states, respectively, T is the temperature $\nu_J = \nu_0 \pm 4B_0(J + 3/2)$ is the frequency of the RRS lines, B_0 is the rotational constant of the molecule, q_J is the statistical weight caused by the nuclear spin, E_J is the rotational energy approximated by the formula $E_J = J(J + 1)hcB_0$; $b_{J\to J'}$ is the Placzek-Teller coefficient. For Stokes and anti-Stokes lines, respectively, they take the form

$$b_{J\to J+2} = \frac{3(J+1)(J+2)}{2(2J+1)(2J+3)}, \quad (18)$$

$$b_{J\to J-2} = \frac{3J(J-1)}{2(2J+1)(2J-1)}. \quad (19)$$

The constants B_0, q_J for the molecules N_2, O_2, and CO_2 are presented, for example, in Ref. 31. It follows from Eq. (17) that the intensity of the RRS lines depends on temperature. This fact is used in the problems of laser sounding. Indeed, if Eq. (17) is written for two allowed transitions J_1 and J_2 their ratio represents the functional dependence on temperature:

$$R(T) = \frac{I_R(J_1,T)}{I_R(J_2,T)} = \exp(\gamma/T + \beta), \quad (20)$$

where

$$\gamma = \left[E_J(J_2) - E(J_1)\right]/k; \ \beta = \ln(b_{J\to J_1} / b_{J\to J_2}).$$

In modeling the Raman scattering angle, some specific peculiarities appear. The angular dependence of the intensity of molecular scattering can be written in the form[26]:

$$I(\vartheta) = I(\pi/2)\left[1 + \chi_{n,p}\cos^2(\vartheta)\right], \quad (21)$$

where, for natural light, $\chi_n = (1 - \rho)/(1 + \rho)$, and for linearly polarized $\chi_p = -(1 - \rho)$. The degree of depolarization is the function of all three invariants of the scattering tensor. Using the known formulas for ρ, it is easy to obtain the relationships for the scattering phase function $g(\vartheta)$. For the frequency-unshifted Cabannes line at excitation by natural light

$$g_S(\vartheta) = K_n^C\left(1 + \frac{180 + \varepsilon}{180 + 13\varepsilon}\mu^2\right), \quad (22)$$

by linearly polarized light

$$g_S(\vartheta) = K_p^C\left(1 - \frac{180 - \varepsilon}{180 + 7\varepsilon}\mu^2\right), \quad (23)$$

for the shifted spectrum of Raman radiation at excitation by natural light

$$g_R(\vartheta) = K_n^R\left(1 + \frac{1}{13}\mu^2\right) \quad (24)$$

and by linearly polarized light

$$g_R(\vartheta) = K_p^R\left(1 - \frac{1}{7}\mu^2\right), \ \mu = \cos(\vartheta). \quad (25)$$

Here K_{np}^{CR} are the normalization constants leading Eqs. (22)–(25) to the form of the probability density. According to the data,[28] the anisotropy factor of the scattering molecule in the Earth's atmosphere $\varepsilon \approx 0.222$. Taking into account the obtained relationships, the logical scheme of modeling the Raman scattering is determined as follows. When realizing the next ith part of the Markovian chain of random collisions of the photon $k(x_{n-1}, \lambda_0 \to x_n, \lambda_0)$, the type of physical interaction is determined on the basis of the weighting relationships of the coefficients in Eq. (3). In the considered model they are the possible variants of scattering of the photon on aerosol or cloudy particles, or on the molecular density fluctuations of the medium. The probability of Raman scattering is not included in the random process of selection because of relatively small value of $\sigma_R \ll \sigma_S$. So, in the case of molecular scattering, further process of random walk bifurcates; radiation appears at the regular set of lines of rotational and vibrational Raman spectrum (see Fig. 1) in addition to the secondary radiation at the frequency λ_0 of incident radiation.

We select the lines of the set of lines of RRS and VRS, which are of practical interest in laser sounding of meteorological parameters of the atmosphere. In the considered numerical experiment they are two lines of RRS and lines of VRS of nitrogen, ozone, and water vapor. Including the determined act of appearance of photons of Raman frequency into the stochastic procedure of selection leads to the shift of the estimate, which is compensated for by the weight method taking into account small probabilities of these events according to Eq. (14). In the examples presented below this value is $\bar{q}_0 \approx 0.036$. After break of the Raman trajectories, the process returns to the point (x_n, λ_0) and continues following the traditional way.

As was mentioned above, one should take into account that, according to expressions (22)–(25), the molecular scattering phase function depends on the photon polarization. In this case, we assumed that laser radiation is linearly polarized. Hence, if the act of molecular scattering has been first ($n = 1$), in modeling the scattering angle, it is necessary to use the formulas (23), (25). If contrary ($n > 1$), the formulas (22), (24) should be used, and it is inessential, which physical character was characteristic of the preceding collisions.

Results of the model calculations

Calculations of the Raman signal under conditions of a cloudy atmosphere taking into account multiple scattering are very few,[32–35] and the results are discrepant. A number of known estimates are presented in Fig. 2 in the form of the relative contribution of the multiple scattering

$$F_M(h) = P^{MS}(h) / P^{SS}(h), \qquad (26)$$

where $P^{SS}(h)$ is the signal of single inelastic Raman scattering, $P^{MS}(h)$ is the multiply scattered component of the signal caused by all types of interaction.

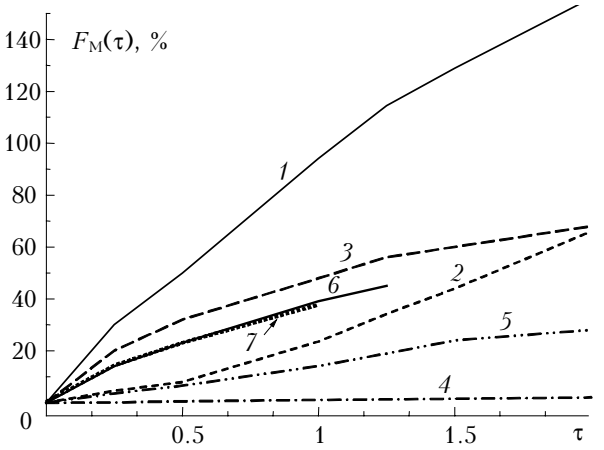

Fig. 2. Comparison of the test calculations of the factor of multiple scattering $F_M(h)$ with the data of other authors: (*1*, *2*) are the results from Ref. 32 and our calculations for the C1 cloud model at the height of 5 km ($\lambda_0 = 308$ nm, $\sigma_S = 10$ km^{-1}); (*3*, *4*, *5*) are the results from Refs. 33 and 35 and our calculations for the same cloudiness model ($\lambda_0 = 532$ nm), (*6*, *7*) are the results from Ref. 34 and our calculations for the model of crystal cloud at the height of $h = 7$–10 km ($\lambda_0 = 355$ nm, $\sigma_S = 0.6$ km^{-1}).

Then, let us call the characteristic $F_M(h)$ the factor of multiple scattering. The majority of calculations, including our own, were performed for a ground-based lidar with the source divergence angle of $\varphi_i = 0.1$ mrad and the full angle of receiving $\varphi_d = 0.4$ mrad. The estimates were obtained for the generally used C1 cloud model[36] at the height $h_0 = 5$ km, having the thickness $\Delta h = 200$ m and the total scattering coefficient $\sigma = 10$ km^{-1}.

It is seen from Fig. 2 that, according to different estimates, the factor $F_M(h)$ varied within quite wide limits. The maximum values (curve *1*) are obtained using the approximate analytical method[32] for $\lambda = 308$ nm. The lowest values of $F_M(h)$ are obtained in calculations[33] by the Monte Carlo method (curve *4*) for the wavelength $\lambda = 532$ nm, the relative addition of multiple scattering does not exceed 2% along the entire sounding path. Our estimates are intermediate. Curves *2* and *5* are calculated, respectively, for $\lambda = 308$ and 532 nm, quantitative behavior of the dependences $F_M(h)$ we obtained does not go out of the limits of similar calculations in Ref. 37, as well as that obtained by different authors for the case of elastic scattering and generalized in Ref. 38. The results by Reichardt[34] (curve *6*) obtained for the model of crystal cloud at $\lambda = 532$ nm are the most close to our estimates (curve *7*).

One of the possible reasons of the discrepancy of the results shown in Fig. 2 is the fact that many authors did not take into account the differences between Rayleigh and Raman scattering phase functions. To illustrate this moment, Figure 3 shows the vertical behavior of the factor of multiple scattering for two models of the scattering phase function $g(\mu)$, (23) and (25), respectively.

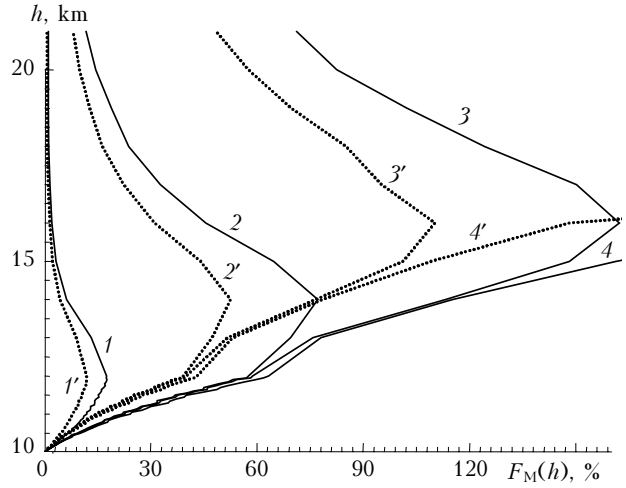

Fig. 3. Vertical profile $F_M(h)$ for two models of the molecular scattering phase functions: Raman (solid lines) and Rayleigh (doted lines). Curves *1–4* are calculations for the receiving angles φ_d = 0.2; 0.4; 0.6; 1 mrad. The model used is a layer of crystal cloud with τ = 0.5 at the height of 10 km, λ_0 = 532 nm.

The estimates are presented for the case of sounding a homogeneous crystal cloud in the height range h = 10–12 km at the frequency of rotational spectrum of N_2, λ = 532 nm. The model profiles of aerosol and molecular scattering here and below correspond to the mean-cyclic model,[39] and the optical characteristics of cloud consisting of chaotically oriented hexagonal columns of mean size are presented in Ref. 40. Comparison of the curves *1–4* with *1′–4′* calculated with the Raman scattering phase function $g^R(\mu)$ and molecular $g^m(\mu)$, respectively, shows that the false choice of model of the Raman scattering phase function can lead to the noticeable shift of the results on the estimated $F_M(h)$. Besides, the behavior of the curves in Fig. 3 demonstrates strong effect of the receiving aperture φ_d on the level of $F_M(h)$. Insignificant expansion of the receiving angle in the limits φ_d = 0.2–1.0 mrad leads to the increase of the factor of multiple scattering by more than 100%. Let us note some qualitative peculiarities of the behavior of $F_M(h)$ with respect to the problem of elastic scattering.

First, the relative level of multiple scattering in the Raman channel is a few lower than that in the channel of elastic scattering at the exciting frequency, in contrast to the results from, for example, Ref. 32. Comparison made for the same problem of sounding of a C1 cloud is shown in Fig. 4.

The reason why we have such situation will be clear if we consider the known analytical estimate[22,25] of the local flux in the detector domain D:

$$\xi \sim \frac{g(\mu^*)\exp[-\tau(\mathbf{r},\mathbf{r}^*)]}{2\pi|\mathbf{r}-\mathbf{r}^*|^2}, \qquad (27)$$

where $\mu^* = (\mathbf{r}^* - \mathbf{r})/|\mathbf{r}^* - \mathbf{r}|$, $\mathbf{r}^* \in D$, $\mathbf{r}(x, y, z)$ is the current point of the scattering event. The value of the normalized scattering phase function $g(\mu)$ is involved in Eq. (27) in explicit form. In acts of single scattering determining the statistical estimate $P^{SS}(h)$, which is in the denominator of expression (26), the value $g_R(\pi \pm \Delta\mu) > g_M(\pi \pm \Delta\mu)$, where $\Delta\mu \le \cos(\varphi_d/2)$ is the small value, and the index M is related to the case of Mie particles. Then the conditions of formation of the multiply scattered component of the signal in the channels of elastic and inelastic scattering are approximately equivalent.

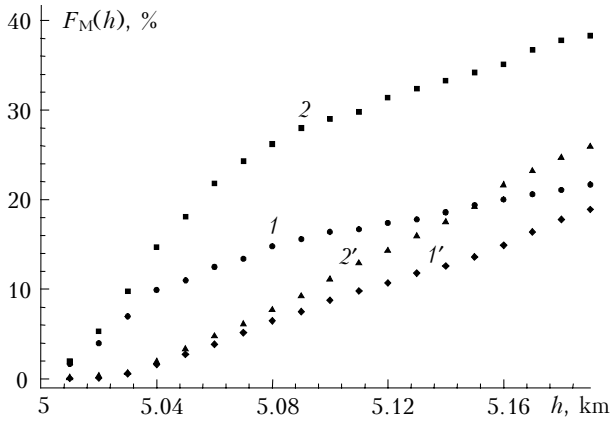

Fig. 4. Comparative level of $F_M(h)$ in the lidar signals of elastic (*1*, *2*) and inelastic (*1′*, *2′*) scattering. Curves *1*, *1′* and *2*, *2′* are calculations for the receiving angles φ_d = 0.2 and 0.4 mrad. Model is C1 cloud, h_0 = 5 km, λ_0 = 532 nm.

Second, the repeatedly noted effect of asymmetry of the scattering phase function is kept. It is related mainly to the fact that at scattering on molecules, different from Mie particles, directions of motion of the photons forward and back are equiprobable. And the contribution of secondary scattered trajectories of the photons in the direction toward the source at high asymmetry of $g(\mu)$ is proportional to $g(\mu \sim 1)$. The increase of the factor $F_M(h)$ as asymmetry of $g_M(\mu)$ increases can be noted when comparing curves *5* and *6* in Fig. 2, obtained for a liquid-droplet cloud with mean particle radius ~ 5 μm and a crystal cloud with hexagonal columns of the height ~ 50 μm. The effect is also seen at less differences in $g_M(\mu)$. The results of calculation of $F_M(h)$ for the test problem "cloud C1" are shown in Fig. 5, with the scattering phase function at the wavelengths of λ_1 = 308 nm (curves *3*, *4*), λ_2 = = 532 nm (curves *1*, *2*), and λ_3 = 1060 nm (curve *5*).

The values of the normalized scattering phase functions at the wavelengths λ_1 and λ_2 in the directions $\vartheta \sim 0°$ differ from that at λ_3 by approximately 8 and 4 times, respectively.

Third, the effect of long-term "afteraction" of the cloud on the shape of the lidar return signal is qualitatively new. As follows from the comparative analysis of the curves $F_M(h)$ in Fig. 3, the effect of the background formed in the cloud layer of the finite length Δh = 10–12 km is kept at the distances exceeding the cloud thickness. Under certain conditions the position of the maximum of $F_M(h)$ is far out of the upper boundary of the cloud.

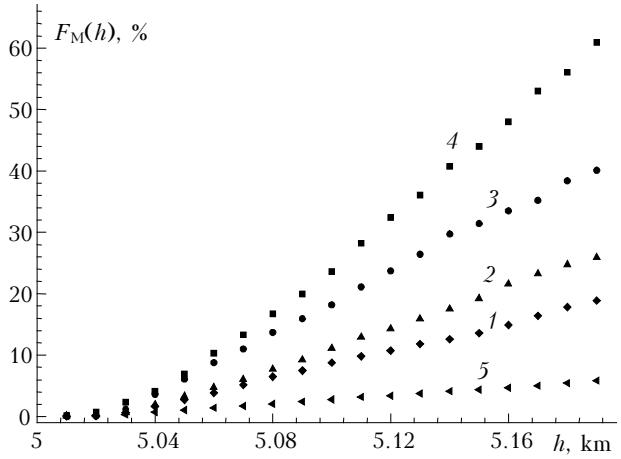

Fig. 5. The effect of asymmetry of the scattering phase function on the level of $F_M(h)$ in the channel of Raman (RRS) scattering calculated at the wavelengths of λ = 532 nm (*1*, *2*), 308 nm (*3*, *4*), and 1060 nm (*5*) and the receiving angles φ_d = 0.2 mrad (*1*, *3*) and 0.4 mrad (*2*, *4*, *5*). The model used is a C1 cloud at the height of h_0 = 5 km.

Then, comparing curves *1–3* in Fig. 3, we see that it is shifted along the depth as the receiving aperture φ_d increases. In the case of elastic scattering[38,41] such an effect is observed, especially in the case of sounding from a satellite,[38] but not to a significant degree.

We assume that the reason for this lies in screening of the single Raman scattering signal by extinction of the incident radiation by more dense cloudy layer according to Bouguer law and extremely low probability of the secondary Raman scattering.

The screening effect of the cloudy layers of different optical thickness is illustrated in Fig. 6. It shows the Raman lidar return $P^R(h)$ recorded within the angular aperture φ_d = 0.4 mrad depending on the depth of the sounded volume in the medium.

Calculations are presented for two sounding diagrams: ground-based (*a*) and satellite (*b*). Curves *1* are calculated for clear atmosphere, i.e., in the absence of a cloudy layer. Curves *2* and *3* correspond to the presence of cloudy layers of the optical thickness τ = 0.5 and 1.

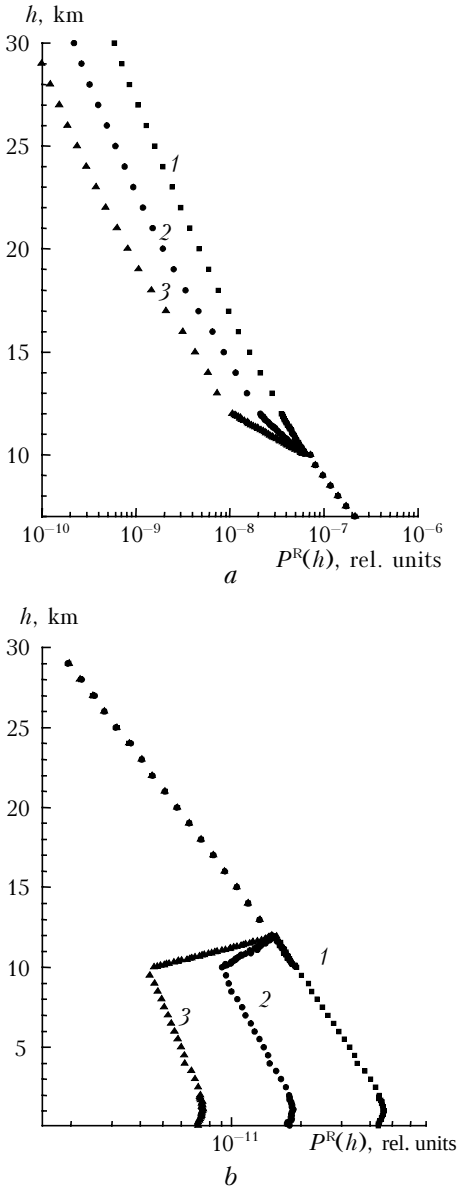

Fig. 6. The effect of screening of the Raman return signal depending on the optical thickness of the cloudy layer for two cases of the lidar sounding – ground-based lidar (*a*) and satellite-borne (*b*). Curves *1*, *2*, and *3* present results calculated for the optical densities of the cloudy layer τ = 0, 0.5 and 1, respectively, the receiving angle φ_d = 0.4 mrad. The model used is a crystal cloud at the heights h_0 from 10 to 12 km above the Earth's surface, λ_0 = 532 nm.

As is seen, the screening effect of the cloudy layer at the level $P^R(h)$ increases as the optical thickness of the cloudy layer increases.

Conclusion

The peculiarities of statistical modeling of transspectral processes accompanying propagation of the laser signal, in particular Raman scattering, require certain modification of the traditional algorithms.

Spectral closeness of the Raman channels of sounding makes it necessary to use correlated sampling; some difficulties appear at modeling of the Cabannes and Raman scattering phase functions due to their ambiguous dependence on the conditions of excitation. The tests of the developed algorithms have shown that the obtained estimates do not contradict the few known data calculated by other authors.

The performed technical calculations allow one to draw preliminary conclusions about some peculiarities in the formation of the background in the channels of inelastic Raman scattering. In particular, the strong effect is observed of afteraction of the cloudy layer on the temporal behavior of the signal. The problem of the effect of multiply scattered component of the Raman-lidar return signal on the accuracy of reconstruction of the specific meteorological parameters (temperature, humidity, etc.) will be considered in the second part of the paper.

Acknowledgments

The work was supported in part by CRDF (grant No. RG2-2357-TD-2).

References

1. G.M. Krekov, S.I. Kavkyanov and M.M. Krekova, *Interpretation of the Signals of Optical Sounding of the Atmosphere* (Nauka, Novosibirsk, 1987), 185 pp.
2. D.V. Pozdnyakov, A.V. Lyaskovskii, H. Grassl, and L. Peterson. Issled. Zemli iz Kosmosa, No. 5, 3–15 (2000).
3. S. Sathyendranath and T. Platt, Appl. Opt. **37**, 2216–2227 (1998).
4. S.H. Melfi, Appl. Opt. **11**, 1605–1610 (1972).
5. D.N. Whiteman, Appl. Opt. **42**, 2571–2608 (2003).
6. R.M. Measures, *Laser Remote Sensing* (John Wiley and Sons, New York, 1987).
7. J. Gelbwachs and M. Dirnhaum, Appl. Opt. **12**, 2442–2447 (1973).
8. E.S. Fry, Y. Emery, X. Quan, and J.W. Katz, Appl. Opt. **36**, 6887–6894 (1997).
9. E.D. Mishina, T.V. Misurgaev, A.A. Nikulin, V.R. Novak, Th. Rasing, and O.A. Aktsipetrov, J. Opt. Soc. Amer. B **16**, 1692–1696 (1999).
10. K.V. Chance and J.D. Spurr, Appl. Opt. **36**, 5224–5229 (1997).
11. J. Rosenberg, A. Ansmann, J. Baldasano, D. Balis, C. Bockmann, B. Calpini, A. Chaicovsky, and P. Flamant, in: *Abstracts of Reports at the 20th International Laser Radar Conference*, Vichy, France (2000), pp. 171–173.
12. V.V. Zuev, A.V. El'nikov, and V.D. Burlakov, *Laser Sounding of the Middle Atmosphere* (Rasko, Tomsk, 2002), 352 pp.
13. S.H. Melfi, D.N. Whiteman, and R.A. Ferrare, J. Appl. Meteorol. **28**, 789–806 (1989).
14. R.A. Ferrare, S.H. Melfi, D.N. Whiteman, and K.D. Evans, Geophys. Res. Lett. **19**, 1599–1602 (1992).
15. S.V. Merkur'ev, V.E. Privalov, and V.G. Shemanin, Pis'ma Zh. Tekh. Fiz. **26**, 45–49 (2000).
16. D. Muller, U. Wandinger, and A. Ansmann, Appl. Opt. **38**, 2358–2368 (1999).
17. A. Ansmann, M. Riebessel, C. Weitkamp, E. Voss, W. Lachmann, and W. Michaelis, Appl. Opt. **55**, 18–28 (1992).
18. C.M.R. Platt, R.T. Austin, S.A. Young, and A.J. Heumsfild, J. Atmos. Sci. **59**, 3145–3173 (2002).
19. K.N. Liou, Mon Weather Rev. **114**, 1167–1195 (1986).
20. V.M. Zakharov, ed., *Laser Sounding from Space* (Gidrometeoizdat, Leningrad, 1988), 215 pp.
21. D.M. Winker, R.H. Couch, and M.P. McCormic, Proc. IEEE **84**, 164–180 (1996).
22. G.I. Marchuk, ed., *Monte Carlo Method in Atmospheric Optics* (Springer-Verlag, Berlin–Heidelberg, 1980), 206 pp.
23. U. Fano, L. Spenser, and M. Berger, *Gamma-Radiation Transfer* (Gosatomizdat, Moscow, 1963), 284 pp.
24. H. Greenspan, ed., *Computing Method in Reactor Physics* (Gordon and Breach Sci. Publ., New York–London–Paris, 1972), 372 pp.
25. G.G. Matvienko, V.V. Veretennikov, G.M. Krekov and M.M. Krekova, Atmos. Oceanic Opt. **16**, No. 12, 1013–1019 (2003).
26. S. Kelikh, *Molecular Nonlinear Optics* (Nauka, Moscow, 1981), 672 pp.
27. A. Behrendt, T. Nakamura, M. Onishi, R. Baumgardt, and T. Tsuda, Appl. Opt. **41**, 7657–7666 (2002).
28. G.W. Kattavar and A.T. Young, Astrophys. J. **242**, 1049–1054 (1981).
29. T.J. Hampreus, G.W. Kattawar, and A.T. Yong, Appl. Opt. **23**, 4422–4426 (1984).
30. D.R. Bates, Planet Space Sci. **32**, 785–790 (1984).
31. C.M. Penney, R.L. Peters, and M. Lapp, J. Opt. Soc. Am. **64**, 712–716 (1974).
32. U. Wandinger, Appl. Opt. **37**, 417–427 (1998).
33. M. Wengenmayer, A.Y.S. Cheng, P. Volger, and U.G. Oppel, Proc. SPIE **5059**, 200–211 (2003)
34. J. Reichardt, Appl. Opt. **39**, 6058–6071 (2000).
35. P. Bruscaglioni, M. Gai, and A. Ismaelli, in: *Proc. of MUSCLE 10*, Florence, Italy (1999), pp. 206–212.
36. D. Deirmendjian, *Electromagnetic Waves Scattering on Spherical Polydispersions* (American Elsevier, New York, 1969).
37. G.G. Matvienko, G.M. Krekov, and M.M. Krekova, in: *Proc. of MUSCLE 10*, Florence, Italy (1999), pp. 157–164.
38. L.R. Bissonette, P. Bruscaglioni, A. Ismaelli, G. Zaccanti, A. Cohen, J. Benayahu, M. Kleiman, S. Egert, C. Flesia, and A.V. Starkov, Appl. Phys. **60**, 355–362 (1995).
39. V.E. Zuev and G.M. Krekov, *Optical Models of the Atmosphere* (Gidrometeoizdat, Leningrad, 1986), 256 pp.
40. G.M. Krekov, M.M. Krekova, D.N. Romashov, and V.S. Shamanaev, Izv. Vyssh. Uchebn. Zaved., Fizika **44**, No. 11, 56–66 (2001).
41. V.V. Belov and A.B. Serebrennikov, Appl. Phys. **75**, 563–570 (2002).